Behavior of double emulsions in a cross-type optical separation system

ARTICLE *in* LANGMUIR · DECEMBER 2014

Impact Factor: 4.46

Kyungheon Lee
Massachusetts General Hospital

Sang Soo Kim
Korea Advanced Institute of Science and Tec…

Hyung Jin Sung
Korea Advanced Institute of Science and Tec…

Langmuir

Article

pubs.acs.org/Langmuir

Behavior of Double Emulsions in a Cross-Type Optical Separation System

Kyung Heon Lee, Sang Bok Kim, Sang Youl Yoon, Kang Soo Lee, Jin Ho Jung, and Hyung Jin Sung*

Department of Mechanical Engineering, KAIST, 291 Daehak-ro, Yuseong-gu, Daejeon, 305-701, Korea

ABSTRACT: The behavior of double emulsions in a cross-type optical particle separation system was studied for different combinations of refractive indices and different inner and outer layer radii. The radii and refractive indices of the double emulsions were easily adjusted by taking advantage of the coflowing geometry of a cross-type optical particle separation device. An analytical expression of the optical forces on a pair of concentric spheres was derived using the photon stream method in the ray optics regime. The predicted trajectories of the double emulsions by the optical force agreed well with the experimental data. This work has potential uses in cell separation by morphometry, drug delivery vehicle, and emulsion-based biomedical applications.

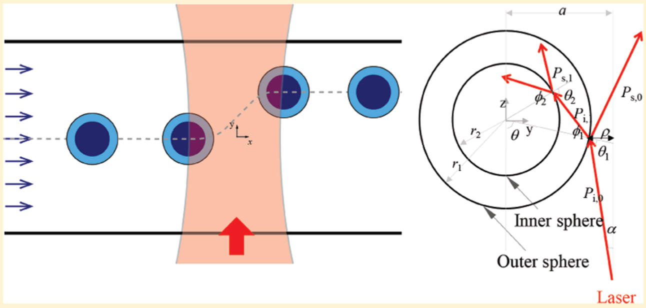

■ INTRODUCTION

Optical forces are used in a variety of fields. Their noninvasive nature has been exploited in the manipulation and separation of microscale biological samples, such as cells,[1] proteins,[2] and biomolecules.[3] Optical beams can apply extremely small forces (on the order of piconewtons)[4] and implement displacement on the order of nanometers,[5] providing a useful tool for the study of macromolecular interactions in soft condensed matter physics.[6] As the need for optical forces has grown, a variety of theoretical schemes have been developed to analyze and design optical manipulators and separators. Among these, the ray optics model is the most successful theoretical approach to optical particle separation and is employed in optical chromatography[7,8] and cross-type optical particle separation devices.[9,10] The ray optics model describes the optical forces that act on objects larger than the wavelength of the illumination beam, which is common in optical particle separation systems.[11]

Because optical chromatography and cross-type optical particle separation use a loosely focused laser beam, the techniques can separate many particles and prevent radiation-induced damage to a sample. Optical scattering forces act to oppose the direction of fluid flow in optical chromatography, in contrast with the optical scattering forces applied in cross-type optical particle separation, which act perpendicular to the direction of fluid flow. Figure 1 shows a schematic diagram of the cross-type optical particle separation. Since size difference and relative refractive index between particle and medium adjust optical force on the particle, the optical force repels the particle away from its origin position along the optical axis with its own properties. The retention distance implies the lateral distance caused by the optical scattering force when the laser is illuminated perpendicular to the flow direction.[10,12] Since the laser is illuminated perpendicular to the particle carrying fluid flow, particles can be continuously separated in a cross-type optical particle separation system.[12]

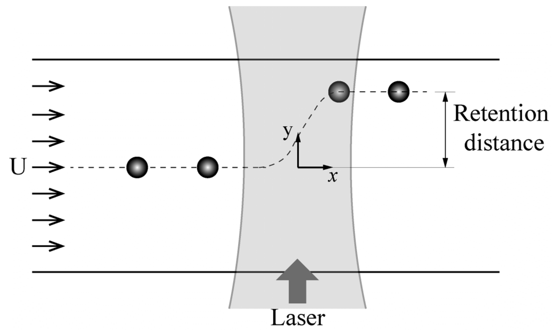

Figure 1. Schematic diagram of the cross-type optical particle separation (COPS).

In the present study, the behavior of double emulsions in a cross-type optical particle separation system was analyzed theoretically and experimentally. A double emulsion shown in Figure 2a was widely used as a microreactor for biochemical reactions, multicomponent microparticles for containing polymerization processes, and encapsulation chambers for drug delivery.[13−18] Double emulsions can be also used as a model of cells to approximate the nucleus and cytoplasm layers. The trajectory of a pair of double emulsions moving in and out of a laser beam was measured experimentally and predicted by solving for the optical forces using a ray optics model and the particle dynamic equations. The generation and measurement of a double emulsion in a cross-type optical particle separation system were conducted simultaneously. The refractive indices

Received: February 17, 2012
Revised: April 21, 2012

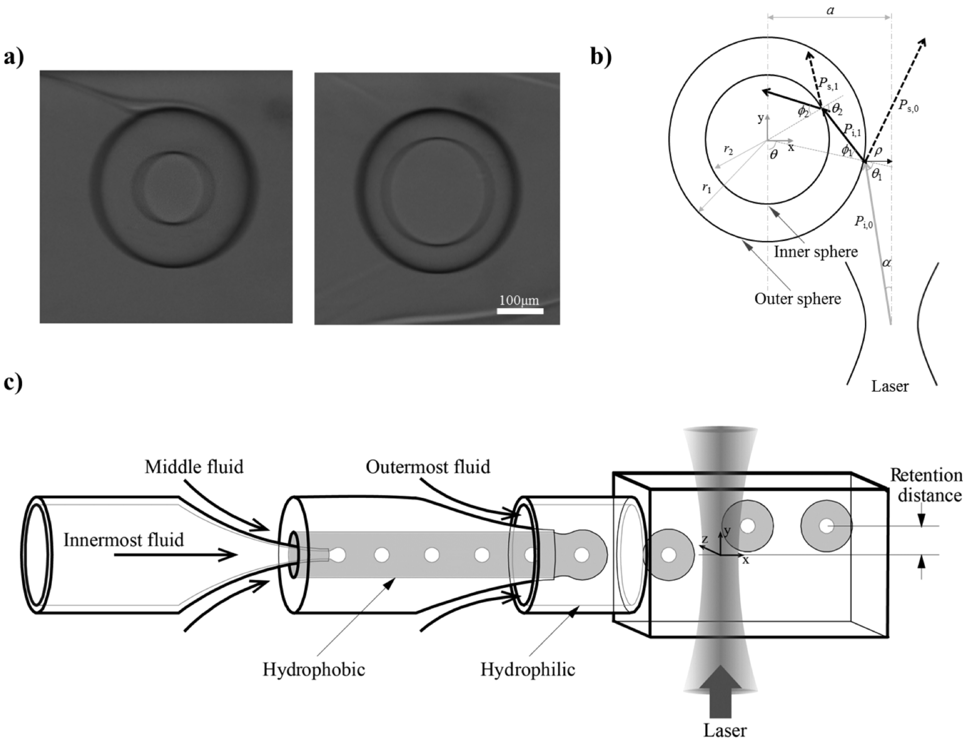

Figure 2. (a) Experimentally generated double emulsions. (b) Schematic diagram of the optical ray stream path. (c) Schematic diagram of the coflowing double emulsion generation device. The scale bar indicates 100 μm.

and relative sizes of the inner and outer emulsions were found to affect the optical force, and these effects were examined closely as a function of the retention distance. The analytical predictions qualitatively agreed well with the experimental measurements. The present results can be applied to the sorting and detection of cells by their morphological difference and encapsulated drug delivery vehicles by their optical property distribution of inner and outer layers.

THEORY

The theoretical calculations using a ray optics model relied on a reference frame in which concentric spheres flowed in a square duct with a channel mean flow velocity **U**, and a laser of wavelength λ was illuminated vertically onto the sphere with power P and a beam waist radius of ω_0. The ratio of the outer to inner radii was r_2/r_1, and each layer had a different refractive index relative to that of the outermost fluid n_0. In the present study, the photon stream method[19,20] was used to formulate an analytical expression for the optical force acting on a pair of concentric spheres. To evaluate the optical force on the sphere, we must determine the change in the momentum of the photons. As shown in Figure 2b, the scattered momentum of the photons $\mathbf{p}_s$ can be expressed with the incident momentum of the photons $\mathbf{p}_i$ and a factor of conversion Q[9]

$$\mathbf{p}_s = Q\mathbf{p}_i \tag{1}$$

The optical force exerted on a sphere can be expressed from eq 1 and Newton's second and third laws

$$\mathrm{d}\mathbf{F} = -\frac{\Delta \mathbf{p}}{\Delta t}\,\mathrm{d}A = -\frac{(\mathbf{p}_s - \mathbf{p}_i)}{\Delta t}\,\mathrm{d}A = \frac{\mathbf{p}_i(1-Q)}{\Delta t}\,\mathrm{d}A \tag{2}$$

where dA is an infinitesimal area normal to the beam direction and Δt is time. Since it is a loosely focused case, the incident ray can be assumed parallel to the beam axis. Therefore, the conversion factor Q[21] is

$$\begin{aligned}
Q &= Q'\exp(\mathrm{i}\alpha) = \frac{Q_N}{Q_D}\\
Q_N &= (1-2R_1)(1-2R_2)\\
&\quad \exp[-i(\theta_1+\theta+2\theta_2-2\varphi_1-2\varphi_2)] - R_1R_2\\
&\quad \exp[-i(\theta_1+\theta-2\varphi_2)] - R_2(1-2R_1)\\
&\quad \exp[-\mathrm{i}(\theta_1+\theta+2\theta_2-2\varphi_1)] - R_1\\
&\quad \exp[-\mathrm{i}(\theta_1+\theta)]\\
Q_D &= 1 - R_1R_2\exp[-\mathrm{i}2(\theta_2-\varphi_1)] + R_2\exp[\mathrm{i}2\varphi_2]\\
&\quad + R_1(1-2R_2)\exp[-\mathrm{i}2(\theta_2-\varphi_1-\varphi_2)]
\end{aligned} \tag{3}$$

The force can be split into the real and imaginary parts, and they are equivalent to the z and y axis force components. An infinitesimal optical force exerted by a single photon stream is given by

$$\begin{aligned}
dF_{x-y} &= \frac{N}{\Delta t}\frac{h}{\lambda}[(\cos\alpha - \mathrm{Re}\{Q\})\mathbf{y} - (\sin\alpha - \mathrm{Im}\{Q\})\\
&\quad \cos\phi\mathbf{x}]r_1^2\sin\theta\cos\theta_1\,\mathrm{d}\theta\,\mathrm{d}\phi
\end{aligned} \tag{4}$$

where N is the number of photons transported through the ray, h is Planck's constant, λ is the wavelength of the light, and **z** and **r** are the axial and radial unit vectors, respectively. By integrating the relations over the integration bounds that determine the trajectory of the photon stream impinging on the interface between the inner (θ_h) and outer (θ_m) spheres

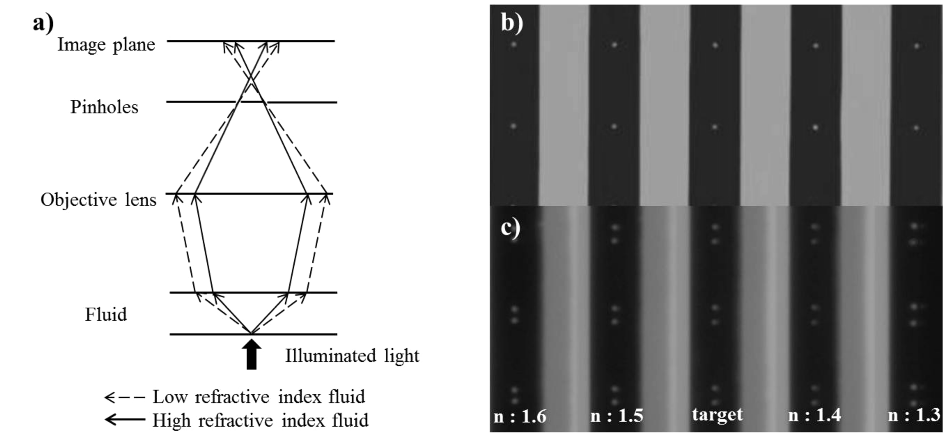

Figure 3. (a) Schematics of the microimage defocusing refractometer. (b) Image spots are on the focal plane. (c) Image spots are out of the focal plane.

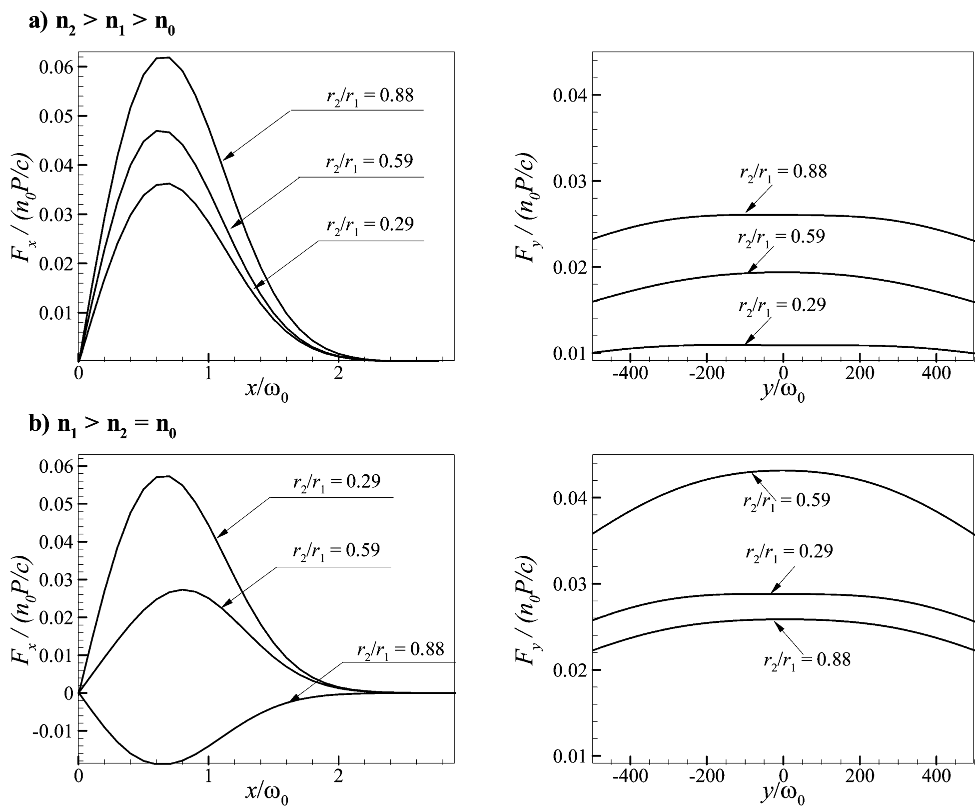

Figure 4. (a) Radial and axial force distributions for $n_2 > n_1 > n_0$ (Case 1: $r_1/\omega_0 = 0.85$, $\lambda/\omega_0 = 5.32 \times 10^{-3}$, $n_1/n_0 = 1.056$, and $n_2/n_0 = 1.106$). (b) Radial and axial force distributions for $n_1 > n_2 = n_0$ (Case 2: $r_1/\omega_0 = 0.85$, $\lambda/\omega_0 = 5.32 \times 10^{-3}$, $n_1/n_0 = 1.106$, and $n_2/n_0 = 1$).

$$\theta_h = \sin^{-1}\left(\frac{n_1}{n_0}\frac{r_2}{r_1}\right) - \alpha \qquad \theta_m = \frac{\pi}{2} - \alpha \tag{5}$$

Then, the axial and radial forces F_y and F_x can be derived as

$$F_y = \frac{n_0}{c} r_1^2 \int_0^{2\pi} \left[\int_{\theta_h}^{\theta_m} I(\rho, y)[\cos\alpha - \mathrm{Re}\{Q_h\}] \sin\theta \cos\theta_1 \, d\theta + \int_0^{\theta_h} I(\rho, y)[\cos\alpha - \mathrm{Re}\{Q\}] \sin\theta \, d\theta \cos\theta_1 \right] d\phi \tag{6}$$

$$F_x = -\frac{n_0}{c} r_1^2 \int_0^{2\pi} \left[\int_{\theta_h}^{\theta_m} I(\rho, y)[\sin\alpha - \mathrm{Im}\{Q_h\}]] I(\rho, y) [\sin\alpha - \mathrm{Im}\{Q_h\}] \sin\theta \cos\theta_1 \, d\theta + \int_0^{\theta_h} I(\rho, y)[\sin\alpha - \mathrm{Im}\{Q\}] \sin\theta \, d\theta \cos\theta_1] \cos\phi \, d\phi \tag{7}$$

■ EXPERIMENTAL SECTION

As shown in Figure 2c, the system we studied included three layers of glass microcapillaries that formed a coflowing geometry,[18,19] which generated a water−oil−water double emulsion. A square glass tube (1

dx.doi.org/10.1021/la300693q | Langmuir XXXX, XXX, XXX−XXX

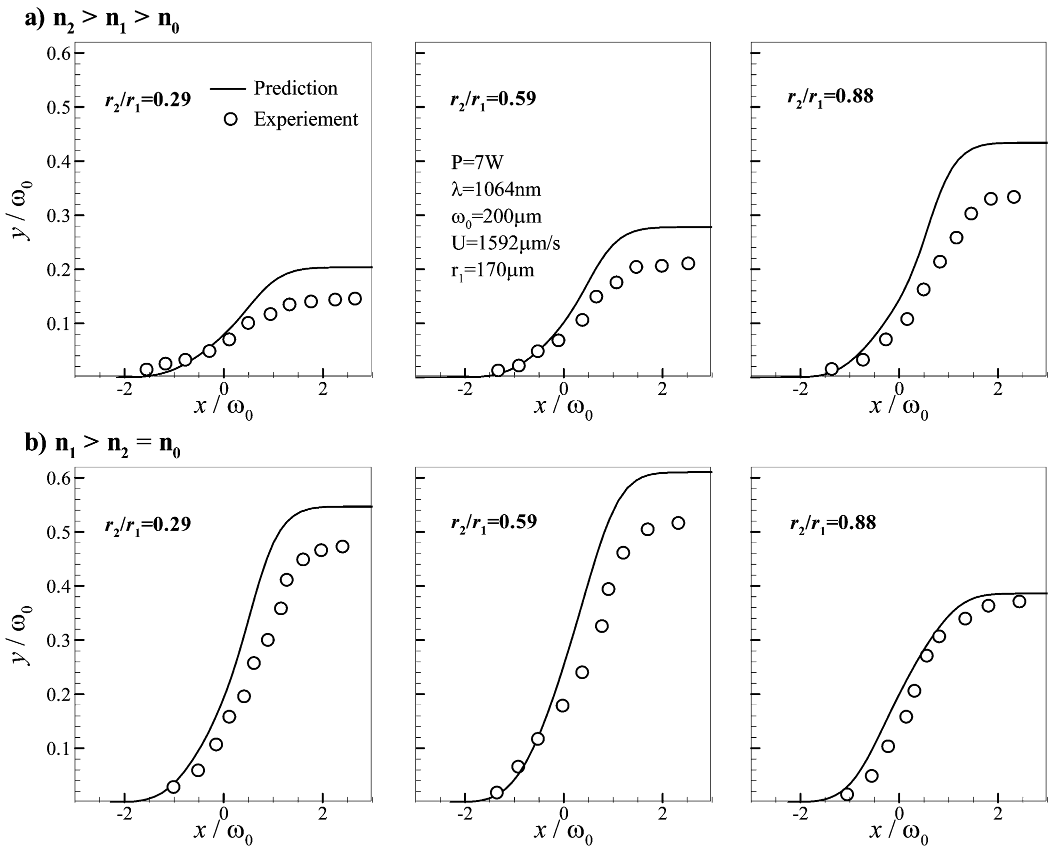

Figure 5. Trajectories for the double emulsions for (a) $n_2 > n_1 > n_0$ and (b) $n_1 > n_2 = n_0$. The laser wavelength was λ = 1064 nm; the beam waist radius was ω_0 = 200 μm.

mm × 1 mm) provided a dynamic observation area in the cross-type optical particle separation system. Because these two components were fabricated on a single device, we generated a double emulsion and simultaneously observed the double emulsion behavior in the presence of optical forces. The glass microcapillaries were fabricated using the conventional heating and pulling method (inner radius 10−180 μm).

Octadecyl trichlorosilane (Sigma Aldrich) treatment was performed on the inner surface of the middle capillary to prevent the water medium from coating the glass surface.[19] Since middle capillary was treated as a hydrophobic surface, the innermost aqueous medium was emulsified in the middle oleic phase fluid under coaxial flow. The oleic phase emulsion was subsequently emulsified in the outer aqueous fluid. The innermost aqueous medium was encapsulated by an oleic phase droplet at the tip of the middle capillary as the oleic phase emulsions were generated. Each capillary was connected to a pulsation free multichannel syringe pump (Nemesys, Cetoni GmbH) for adjusting the volumetric flow rate of each fluid flow. The net fluid flow rate was about 5700 μL/h and the emulsion velocity in the microchannel was about 1592 μm/s. The outer radius of an emulsion was about 150 μm and the inner radius of an emulsion varied over the range 40−130 μm as a function of the inner and middle fluid flow rates. The aqueous solution of 2 wt % polyvinyl alcohol (Sigma Aldirch) was used for the outermost fluid. Ethoxylated trimethylolpropane triacrylate (Sigma Aldrich, n = 1.470) and polydimethylsiloxane oil (Sigma Aldrich, n = 1.405) were used as the middle oil phase of the water/oil/water double emulsion. $CaCl_2$ was added to aqueous solution to adjust the refractive index at the inner aqueous phase.

We measured the refractive index of a 6 M $CaCl_2$ solution (n = 1.469) using the defocused microrefractometer method.[22] A schematic diagram of the refractometer is shown in Figure 3a. Since the refractive indexes of each reference fluid are different, the refractive angle at the interface of fluid and glass varies with the refractive index of the fluid. When a spot is located on the focal plane, whether two pinhole apertures are in front of the image plane or not, a single spot image appears at the image plane in Figure 3b. In the case of a spot moving away from the focal plane, the spot image is separated as two blurred spot images at the image plane in Figure 3c. The distances between each spot image are determined by the refractive index of the fluid. The device simply consists of five silicon-etched microfluidic channels and 3 μm patterned spots on their bottom glass surfaces, and each channel is filled with reference fluids and target fluid. Since the spot images for all fluids are captured in the same image frame, the refractive index of target fluid can be obtained by simple curve fitting from a single step measurement. In this device, four authorized refractive index fluids n = 1300, 1400, 1500, and 1600 (Cargille Laboratories) were used as reference fluids.

To prevent absorption of 1064 nm light by the water media, heavy water (D_2O) was used as the aqueous phase.[23] The refractive index and diameter of each emulsion layer were adjusted to generate a model for cell-nucleus morphometry systems (Case 1: $n_1 > n_2 > n_0$) using a water/oil/water double emulsion or a hollow sphere (Case 2: $n_1 > n_2 = n_0$). The laser beam waist radius was adjusted using a spherical lens and was illuminated vertically in the direction of the fluid flow. Since the vertical alignment between the incident angle of light and the sidewall of the square capillary was crucial, the device was aligned using a custom-made 5-axis stage for alignment. Since the double emulsions passed the light within a very short time and the optical scattering force was perpendicular to the gravitational force, the influence of the gravitational force on the vertical displacement was negligible.

■ RESULTS AND DISCUSSION

Figure 4 shows the normalized optical force distributions for both cases during the cross-type particle separation. As is true for most biological cells, the inner of the concentric spheres had a larger refractive index than the outer sphere. The refractive index of the cell nucleus is usually higher than that of the cell

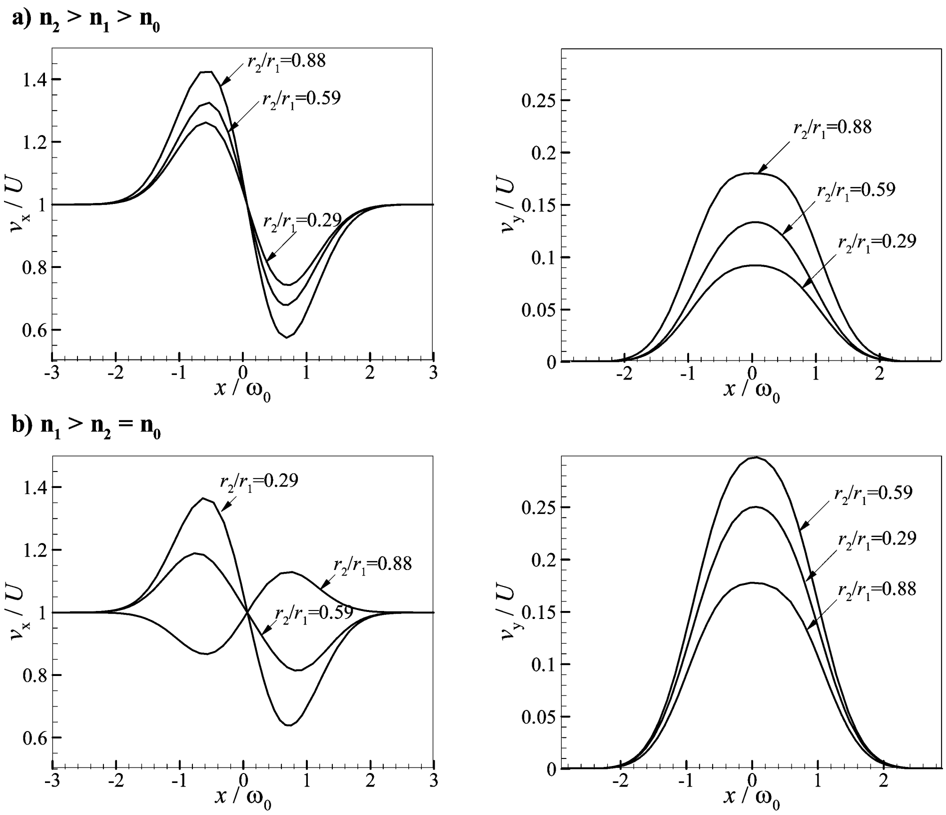

Figure 6. Variations in the velocity of the double emulsions for (a) $n_2 > n_1 > n_0$ and (b) $n_1 > n_2 = n_0$.

cytoplasm.[21,24] For Case 1, the calculations were performed for three ratios of inner to outer sphere radii, $r_2/r_1 = 0.29$, 0.59, and 0.88 in Figure 4a. The axial and radial forces both increased as the inner sphere radius increased. A sphere in which the refractive index of the inner sphere was higher than that of the outer sphere yielded more refracted trajectories for photons that passed through the inner sphere. This meant that more momentum was transferred to the emulsion.

For Case 2, the refractive index ratio was adjusted to $n_1/n_0 = 1.106$, $n_2/n_0 = 1$, which included an outer sphere with a high refractive index and an inner sphere and outer fluid with lower identical refractive indices. As shown in Figure 4b, the optical force distributions differed from those of Case 1. Total internal reflection could explain this unexpected force distribution. Since the refractive index of the inner sphere was smaller than that of the outer sphere, total internal reflection occurred at the interface of the inner sphere. From Figure 2b, the critical angle at the interface between the inner and outer spheres was defined by $\sin \theta_{2,\mathrm{crit}} = n_2/n_1$, which is equivalent to $\sin \theta_{1,\mathrm{crit}} = r_2/r_1$. When the total internal reflection occurred, the photons were totally reflected backward at the interface of the inner sphere so that the axial force increased. As the relative size of the inner sphere decreased, total internal reflection occurred at smaller values of θ_1, and more photons underwent total internal reflection. However, the relative size of the inner sphere increased, and total internal reflection occurred at larger values of θ_1 such that fewer photons underwent total internal reflection. For $r_2/r_1 = 0.88$, the lower refractive index of the inner sphere compared to the outer sphere and the effects of total internal reflection were relatively small because of the large size ratio. The radial force distribution of the laser beam repelled the sphere away from the center axis of the laser beam to a region near the laser beam waist. In the radial force distribution, when the photons underwent total internal reflection, the sphere was pushed away from the beam axis. This pushing effect increased as the relative size of the inner sphere increased, since the critical angle increased as the relative size of the inner sphere increased. As shown in Figure 4b, the pushing effect was dominant at $r_2/r_1 = 0.88$ and the radial force acted in an outward direction from the laser beam axis.

Trajectories of the emulsion in the cross-type particle separation system are experimentally observed and plotted in Figure 5. The predicted trajectories are also shown for comparison. The equations describing the dynamics of double emulsions subject to cross-type optical particle separation can be expressed as[10]

$$m_p \frac{\mathrm{d}r}{\mathrm{d}t} - 6\pi\mu r_p (U - V_p) = F \qquad \mathbf{U} = U\hat{\mathbf{x}}$$
$$\mathbf{V}_p = v_p\hat{\mathbf{x}} + w_p\hat{\mathbf{y}} \quad \mathbf{F} = F_y\hat{\mathbf{y}} + F_x\hat{\mathbf{x}} \tag{8}$$

where m_p is the particle mass, $\mathbf{r}$ is the particle position vector, μ is the dynamic viscosity of the fluid, $\mathbf{F}$ is the optical force vector from eqs 6 and 7, and $\mathbf{U}$ and $\mathbf{V}_p$ are the fluid and particle velocity vectors, respectively. As shown in Figure 5, the experimental data were qualitatively in good agreement with the predicted data, although the experimental values were slightly lower than the predicted values. This small discrepancy was attributed to the fact that both the inner and outer emulsions consisted of only liquid, and their behaviors differed from that of a solid concentric sphere. If two liquids had relatively high mutual solubility or low mutual solubility but were generated a long time before, the diffusion of two liquids made a graded refractive index interface and the optical force distribution at the graded refractive index interface had a

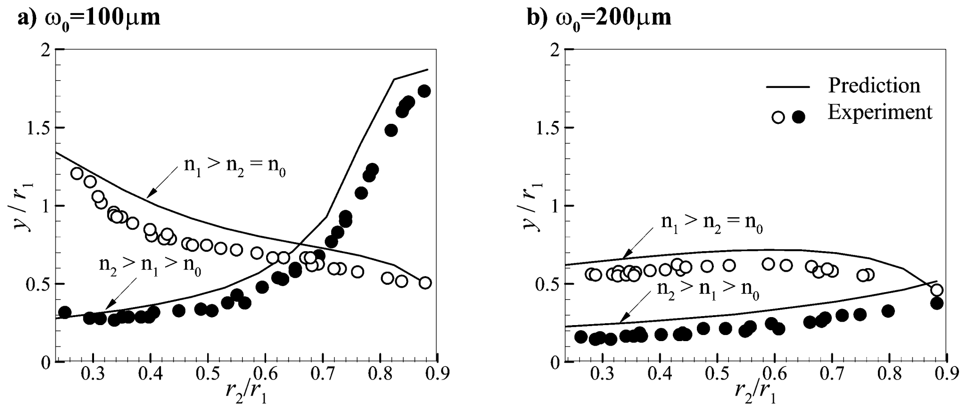

Figure 7. Effect of the retention distance on the ratio of the radii (r_2/r_1) for (a) ω_0 = 100 μm and (b) ω_0 = 200 μm.

different distribution against the sharp interface. However, the mutual solubility of the present study was very low. For Case 1, the retention distance of the double emulsion increased as r_2/r_1 increased in Figure 5a. Because both the gradient and scattering forces on the double emulsions increased in Case 1, as shown in Figure 4a, the retention distance also increased. As mentioned earlier, because the inner emulsion had a larger refractive index, the transferred photon momentum was increased as the size of the inner emulsion increased, as shown in Figure 4a. The different behavior of the emulsion is shown in Figure 5b. For Case 2, the refractive index ratio (n_2/n_1) was smaller than 1; the transferred photon momentum decreased as the inner emulsion radius increased. However, total internal reflection and the angle between the ray and the beam increased the retention distance of r_2/r_1 = 0.59 compared to r_2/r_1 = 0.29, and the smallest retention distance was r_2/r_1 = 0.88.

Numerical simulations permit the decomposition of the double emulsion behavior into each directional velocity component to estimate the dynamics for each direction.[10] Figure 6 shows the velocity components of each case. For Case 1, the velocity distributions in the y and z directions changed significantly as the ratio of the inner to outer emulsion increased. Figure 6a plots the acceleration and deceleration of the emulsion as it passed through the center axis of the laser beam due to each component of the optical force, as shown in Figure 4a. Figure 6b shows different behavior, that is, the gradient force distribution of r_2/r_1 = 0.59 shown in Figure 4b was smaller than that corresponding to r_2/r_1 = 0.29, and the y-directional velocity distribution was small. For r_2/r_1 = 0.88, the radial velocity displayed the opposite behavior as a result of the gradient force distribution, as mentioned earlier.

The effects of the laser beam waist radius on the behavior were investigated by calculating and experimentally measuring the retention distance of a double emulsion for two cases. In the first case, the laser beam waist (ω_0) was larger than the radius of the emulsion (r_1). In the second case, ω_0 was comparable to or smaller than the radius of the emulsion. The retention distance as a function of the ratio of the inner to outer radii is plotted in Figure 7. The experimental measurements agreed well with the theoretical predictions. For Case 1 (ω_0 = 100 μm) shown in Figure 7a, the retention distance increased as the inner radius increased, and it decreased as the inner radius increased for Case 2. In contrast, a different trend was observed for ω_0 = 200 μm, as shown in Figure 7b. The retention distance in Case 1 displayed a similar directional change with increasing inner emulsion radius for both beam waist radii, but the retention distance of ω_0 = 100 μm was larger than that corresponding to ω_0 = 200 μm. As mentioned earlier, the inner emulsion impinging condition (θ_h) increased as the beam waist radius (ω_0) decreased. This meant that more photons could impinge on the inner emulsion surface as the beam waist radius decreased. Additionally, a larger gradient force for smaller beam waist radii lengthened the trapping time for the double emulsion, consistent with the nonlinear behavior of cross-type optical particle separation systems described in our previous study.[25] The retention distances for Case 2, in which total internal reflection occurred at the interface of the inner emulsion, followed a different trend for each beam waist radius. This could be explained in terms of the inner emulsion impinging conditions θ_h. In contrast with Case 1, the lower refractive index of the inner emulsion resulted in total internal reflection at the interface between the inner and outer emulsions.

■ CONCLUSIONS

We experimentally investigated the behavior of the double emulsions in a cross-type optical separation system based on the trajectories and the final retention distance. The behavior of the double emulsion was predicted using the photon stream method and particle dynamic equations. We confirmed that the behavior of the double emulsion in the cross-type optical particle separation system agreed well with the predicted results. The effects of the optical force on the continuous separation of the double emulsion depended on the size of the inner emulsion layer and the refractive index ratio between the inner and outer emulsions. We additionally found that total internal reflection at the interface of the inner emulsion produced complex behavior for water/oil/water double emulsions or hollow spheres. The observed and predicted behaviors of the double emulsions in the presence of optical forces have important implications for cell manipulation, cell-nucleus morphometric models, and emulsion-based drug delivery vehicles.

■ AUTHOR INFORMATION

Corresponding Author

*Tel: 82-42-350-3027. Fax: 82-42-350-5027. E-mail: hjsung@kaist.ac.kr.

Notes

The authors declare no competing financial interest.

dx.doi.org/10.1021/la300693q | *Langmuir* XXXX, XXX, XXX−XXX

■ ACKNOWLEDGMENTS

This work was supported by the Creative Research Initiatives (No. 2012-0000246) program of the National Research Foundation of Korea.

■ REFERENCES

(1) Ashkin, A. Optical trapping and manipulation of neutral particles using lasers. *Proc. Natl. Acad. Sci. U.S.A.* **1997**, *94* (10), 4853.

(2) Svoboda, K.; Schmidt, C. F.; Schnapp, B. J.; Block, S. M. Direct observation of kinesin stepping by optical trapping interferometry. *Nature* **1993**, *365* (6448), 721−727.

(3) Bockelmann, U.; Thomen, P.; Essevaz-Roulet, B.; Viasnoff, V.; Heslot, F. Unzipping DNA with optical tweezers: high sequence sensitivity and force flips. *Biophys. J.* **2002**, *82* (3), 1537−1553.

(4) Footer, M. J.; Kerssemakers, J. W. J.; Theriot, J. A.; Dogterom, M. Direct measurement of force generation by actin filament polymerization using an optical trap. *Proc. Natl. Acad. Sci. U.S.A.* **2007**, *104* (7), 2181.

(5) Greenleaf, W. J.; Woodside, M. T.; Abbondanzieri, E. A.; Block, S. M. Passive all-optical force clamp for high-resolution laser trapping. *Phys. Rev. Lett.* **2005**, *95* (20), 208102.

(6) Grier, D. G. A revolution in optical manipulation. *Nature* **2003**, *424* (6950), 810−816.

(7) Kaneta, T.; Ishidzu, Y.; Mishima, N.; Imasaka, T. Theory of optical chromatography. *Anal. Chem.* **1997**, *69* (14), 2701−2710.

(8) Hart, S. J.; Terray, A. V. Refractive-index-driven separation of colloidal polymer particles using optical chromatography. *Appl. Phys. Lett.* **2003**, *83*, 5316.

(9) Kim, S. B.; Kim, S. S. Radiation forces on spheres in loosely focused Gaussian beam: ray-optics regime. *JOSA B* **2006**, *23* (5), 897−903.

(10) Kim, S. B.; Kim, J. H.; Kim, S. S. Theoretical development of in situ optical particle separator: cross-type optical chromatography. *Appl. Opt.* **2006**, *45* (27), 6919−6924.

(11) Ashkin, A. Forces of a single-beam gradient laser trap on a dielectric sphere in the ray optics regime. *Biophys. J.* **1992**, *61* (2), 569−582.

(12) Kim, S. B.; Yoon, S. Y.; Sung, H. J.; Kim, S. S. Cross-type optical particle separation in a microchannel. *Anal. Chem.* **2008**, *80* (7), 2628−2630.

(13) Leal-Calderon, F.; Schmitt, V.; Bibette, J. *Emulsion science: basic principles*; Springer Verlag: Dusseldorf, 2007.

(14) Lorenceau, E.; Utada, A. S.; Darren, R.; Cristobal, G.; Joanicot, M.; Weitz, D. A. Generation of polymerosomes from double-emulsions. *Langmuir* **2005**, *21* (20), 9183−9186.

(15) Chen, C. H.; Shah, R. K.; Abate, A. R.; Weitz, D. A. Janus particles templated from double emulsion droplets generated using microfluidics. *Langmuir* **2009**, *25* (8), 4320−4323.

(16) Hirai, T.; Hariguchi, S.; Komasawa, I.; Davey, R. J. Biomimetic synthesis of calcium carbonate particles in a pseudovesicular double emulsion. *Langmuir* **1997**, *13* (25), 6650−6653.

(17) Theberge, A. B.; Courtois, F.; Schaerli, Y.; Fischlechner, M.; Abell, C.; Hollfelder, F.; Huck, W. T. S. Microdroplets in Microfluidics: An Evolving Platform for Discoveries in Chemistry and Biology. *Angew. Chem., Int. Ed.* **2010**, *49* (34), 5846−5868.

(18) Utada, A.; Lorenceau, E.; Link, D.; Kaplan, P.; Stone, H.; Weitz, D. Monodisperse double emulsions generated from a microcapillary device. *Science* **2005**, *308* (5721), 537.

(19) Gauthier, R.; Wallace, S. Optical levitation of spheres: analytical development and numerical computations of the force equations. *JOSA B* **1995**, *12* (9), 1680−1686.

(20) Gauthier, R. C. Laser-trapping properties of dual-component spheres. *Appl. Opt.* **2002**, *41* (33), 7135−7144.

(21) Chang, Y. R.; Hsu, L.; Chi, S. Optical trapping of a spherically symmetric sphere in the ray-optics regime: a model for optical tweezers upon cells. *Appl. Opt.* **2006**, *45* (16), 3885−3892.

(22) Yoon, S. Y.; Yang, S. Microfluidic refractometer with micro-image defocusing. *Lab Chip* **2011**.

(23) Dholakia, K.; Reece, P. Optical micromanipulation takes hold. *Nano Today* **2006**, *1* (1), 18−27.

(24) Brunsting, A.; Mullaney, P. F. Differential light scattering from spherical mammalian cells. *Biophys. J.* **1974**, *14* (6), 439−453.

(25) Kim, S. B.; Lee, K. H.; Sung, H. J.; Kim, S. S. Nonlinear particle behavior during cross-type optical particle separation. *Appl. Phys. Lett.* **2009**, *95* (26), 264101−264101−3.